CHIN. PHYS. LETT. Vol. 34, No. 4 (2017) 049701

# Nucleosynthesis in Advection-Dominated Accretion Flow onto a Black Hole *

Jiang Zhang(张江)[1,2**], Ren-Yi Ma(马任意)[3**], Hong-Jie Li(李宏杰)[4], Bo Zhang(张波)[5]

[1]*Department of Mathematics and Science, Hebei GEO University, Shijiazhuang 050016*
[2]*Key Laboratory for the Structure and Evolution of Celestial Objects, Chinese Academy of Sciences, Kunming 650011*
[3]*Department of Astronomy, Xiamen University, Xiamen 361005*
[4]*School of Sciences, Hebei University of Science and Technology, Shijiazhuang 050016*
[5]*Department of Physics, Hebei Normal University, Shijiazhuang 050016*

(Received 15 December 2016)

*Nucleosynthesis in advection-dominated accretion flow (ADAF) onto a black hole is proposed to be an important role in chemical evolution around compact stars. We investigate the nucleosynthesis in ADAF relevant for a black hole of low mass, different from that of the self-similar solution. In particular, the presence of supersolar metal mass fractions of some isotopes seems to be associated with the known black hole nucleosynthesis in ADAF, which offers further evidence of diversity of the chemical enrichment.*

*PACS: 97.10.Cv, 26.40.+r, 97.10.Tk* DOI: 10.1088/0256-307X/34/4/049701

Burbidge *et al.*[1] stated in 1957 that most of the heavy nuclei beyond iron peak are synthesized by the incessant growth of neutrons classified into two basic principal capture processes: the slow neutron-capture process (the s-process),[2] and the rapid neutron-capture process (the r-process).[3] Through decades of extensive research, understanding the nature of nucleosynthesis of heavy elements beyond iron still is one of the largest obstacles in astrophysics and physics.

For the sake of unveiling this long-standing problem, nuclear reaction networks under different conditions, either cold or hot in temperature, are studied. Typical examples of nucleosynthesis network involve proton–proton chains, CNO cycle processes, etc., up to neutron-capture, from low temperatures ($T < 10^8$ K) to higher temperatures. After some nucleosynthesis processes, elemental abundances can be calculated, different from those produced in the corresponding reactions on different astrophysical sites.

The theory of accretion onto a compact star has played essential roles in many fields of modern astrophysics, such as supernovae Ia,[4,5] quasars, x-ray binaries, active galactic nuclei (AGNs), and cataclysmic variable binary star systems. Since Shakura *et al.*[6] proposed the thin accretion disk model in the 1970s, tremendous progress has been made through several decades of extensive research to explain an enormous number of high-energy astrophysical systems. To overcome the problem of optically thin hot accretion disks, Narayan *et al.*[7,8] put forward the advection-dominated accretion flow (ADAF) theory devoid of any thermal instability.

A possible site of nucleosynthesis is believed to be in the hot accretion and outflow regions that stray from black-hole accretion disks.[9] Earlier work[10] revealed an important role for accretion flows around black holes with different masses as the significant nucleosynthesis mechanism for forming various elements from light to heavy. Obviously, among several different sites responsible for the synthesis of elements, this is a non-traditional nucleosynthesis channel distinct from that of core-collapse supernovae. Furthermore, nuclear reaction of free neurons and protons produced from the hot disk would likely synthesize some critical elements, e.g., nickel-56.[11] Unlike previous works, Hu *et al.*[12] calculated nuclear reactions and nucleosynthesis in the accretion flow models from ADAF. However, the work by Hu *et al.* is based on the self-similar solution of ADAF. In contrast to the global solution, the advection factor is simply assumed to be constant, and the transonic condition is not satisfied. As a result, the self-similar solution deviates from the global solution significantly, especially in the inner region of the disk.[7,8] This motivates us to revisit the nucleosynthesis in ADAF onto a black hole.

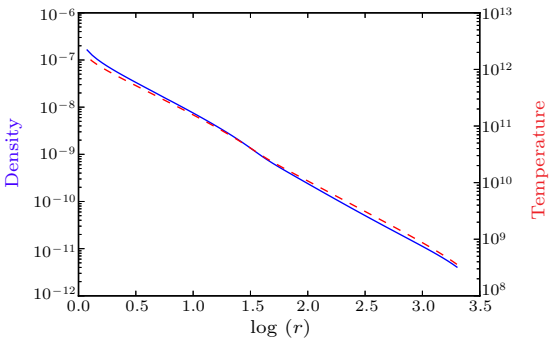


**Fig. 1.** Densities (left vertical axis) and temperatures (right vertical axis) as a function of radius for the $10M_\odot$ black hole. The solid line is the calculated density curve, and the dashed line indicates the temperature of the predictions.

Considering the dynamics of black hole accretion disks, the height-averaged basic equations depicting the ADAF are as follows:

$$\dot{M} = -4\pi r\rho H\upsilon = \text{const}, \tag{1}$$

$$\upsilon\frac{d\upsilon}{dr} = (\Omega^2 - \Omega_{\rm K}^2)r - \frac{1}{\rho}\frac{dp}{dr}, \tag{2}$$

$$\dot{M}\frac{d}{dr}(\Omega r^2) = -\frac{d}{dr}(4\pi r^2\tau_{r\varphi}H), \tag{3}$$

*Supported by the National Natural Science Foundation of China under Grant Nos 11547041, 11403007, 11673007, 11643007, 11333004, U1531130, 11673059, 11390374 and 11521303, and the Chinese Academy of Sciences under Grant Nos KJZD-EW-M06-01 and QYZDB-SSW-SYS001.

**Corresponding author. Email: zhangphysics@126.com

$$\rho\upsilon T_{\rm i}\frac{ds_{\rm i}}{dr}=(1-\delta)q^{+}_{\rm vis}-q_{\rm ie}, \tag{4}$$

$$\rho\upsilon T_{\rm e}\frac{ds_{\rm e}}{dr}=\delta q^{+}_{\rm vis}+q_{\rm ie}-q^{-}, \tag{5}$$

where $\dot{M}$ stands for the accretion rate, $c_{\rm s}\equiv\sqrt{p/\rho}$ stands for the isothermal sound speed, $p=p_{\rm gas}/\beta_{\rm t}=\rho c_{\rm s}^2/\beta_{\rm t}$ stands for the total pressure of the tangled magnetic field and the gas pressure, $\beta_{\rm t}$ stands for the ratio of the gas pressure to the total pressure and is set at its 'typical' value $\beta_{\rm t}=0.9$, $T$ stands for the temperature, and $s$ stands for the entropy. The subscripts i and e denote the quantities for ions and electrons, respectively. The quantity $\tau_{r\varphi}=-\alpha p$ stands for the $r\varphi$ component of the viscous stress tensor using the $\alpha$ prescription,[6] $H=c_{\rm s}/\Omega_{\rm K}$ denotes the vertical scale height, $\Omega_{\rm K}$ denotes the Keplerian angular velocity, $\delta$ is the fraction of the total energy that directly heats the electrons and is fixed to be $\delta=0.3$ in the wake of the detailed modeling result to the supermassive black hole in the Galactic center,[13] $q^{+}_{\rm vis}=r\tau_{r\varphi}(d\Omega/dr)$ represents the heating rate of the viscosity, $q_{\rm ie}$ denotes the volume energy transfer rate from ions to electrons via Coulomb collisions, and $q^{-}$ stands for the cooling rate of the electrons, which involves bremsstrahlung, synchrotron, and Comptonization.

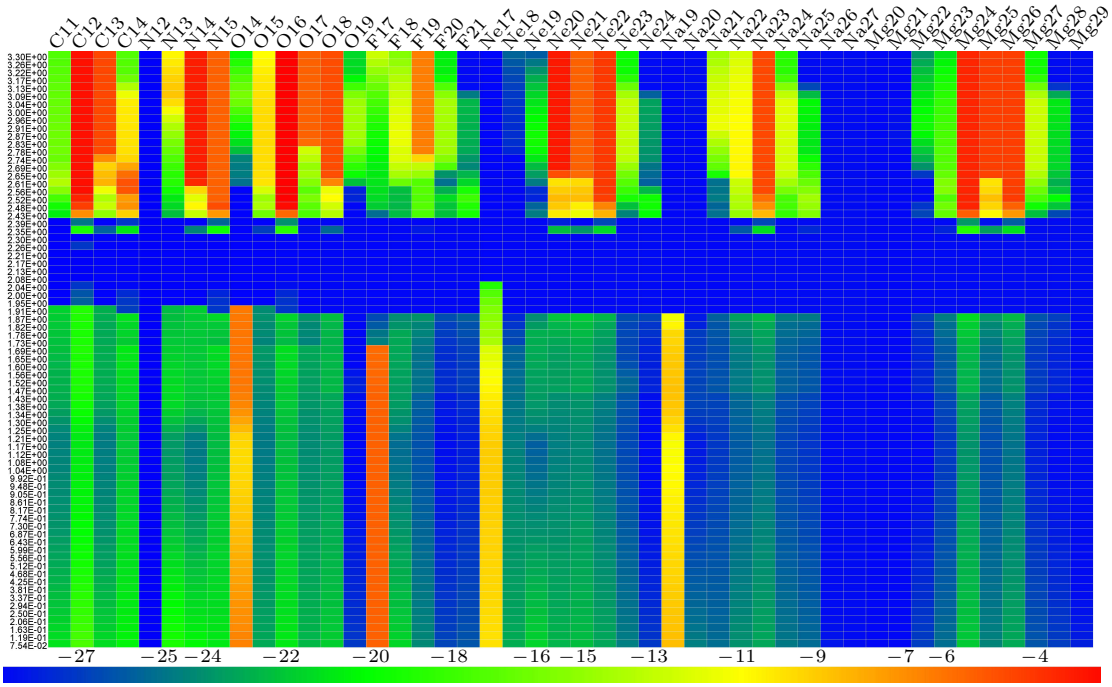


**Fig. 2.** Heat map showing the mass fractions of different isotopes from $^{11}$C to $^{29}$Mg as a dependent variable (horizontal axis) of the radial coordinates (vertical axis) for given black hole mass.

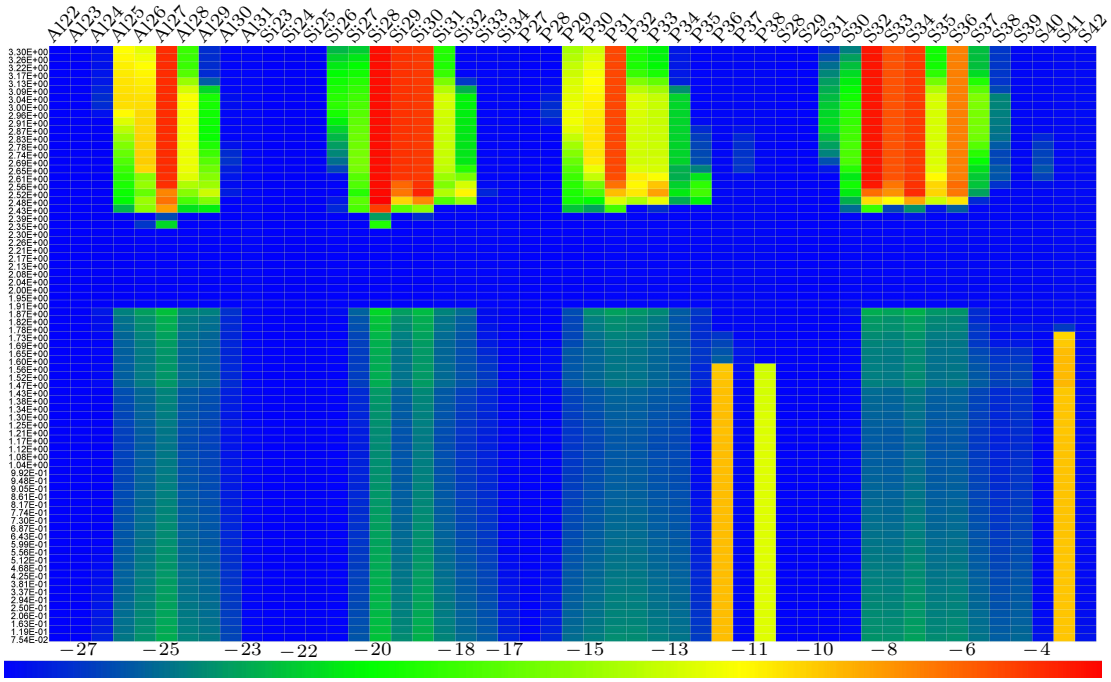


**Fig. 3.** The same as Fig. 2, but for isotopes from $^{22}$Al to $^{42}$S.

**Table 1.** Mass fractions of elements from C to S.

| $\log(r/r_{\rm schw})$ | C | N | O | F | Ne | Na | Mg | Al | Si | P | S |
|---|---|---|---|---|---|---|---|---|---|---|---|
| 3.30E+00 | 3.07E−03 | 1.11E−03 | 9.62E−03 | 4.05E−07 | 1.75E−03 | 3.34E−05 | 6.60E−04 | 5.81E−05 | 7.11E−04 | 8.16E−06 | 4.18E−04 |
| 3.26E+00 | 3.07E−03 | 1.11E−03 | 9.62E−03 | 4.05E−07 | 1.75E−03 | 3.34E−05 | 6.60E−04 | 5.81E−05 | 7.11E−04 | 8.16E−06 | 4.18E−04 |
| 3.22E+00 | 3.07E−03 | 1.11E−03 | 9.62E−03 | 4.05E−07 | 1.75E−03 | 3.34E−05 | 6.60E−04 | 5.81E−05 | 7.11E−04 | 8.16E−06 | 4.18E−04 |
| 3.17E+00 | 3.07E−03 | 1.11E−03 | 9.62E−03 | 4.05E−07 | 1.75E−03 | 3.34E−05 | 6.60E−04 | 5.81E−05 | 7.11E−04 | 8.16E−06 | 4.18E−04 |
| 3.13E+00 | 3.07E−03 | 1.11E−03 | 9.62E−03 | 4.05E−07 | 1.75E−03 | 3.34E−05 | 6.60E−04 | 5.81E−05 | 7.11E−04 | 8.16E−06 | 4.18E−04 |
| 3.09E+00 | 3.07E−03 | 1.11E−03 | 9.62E−03 | 4.05E−07 | 1.75E−03 | 3.34E−05 | 6.60E−04 | 5.81E−05 | 7.11E−04 | 8.16E−06 | 4.18E−04 |
| 3.04E+00 | 3.07E−03 | 1.11E−03 | 9.62E−03 | 4.05E−07 | 1.75E−03 | 3.34E−05 | 6.60E−04 | 5.81E−05 | 7.11E−04 | 8.16E−06 | 4.18E−04 |
| 3.00E+00 | 3.07E−03 | 1.11E−03 | 9.62E−03 | 4.05E−07 | 1.75E−03 | 3.34E−05 | 6.60E−04 | 5.81E−05 | 7.11E−04 | 8.16E−06 | 4.18E−04 |
| 2.96E+00 | 3.07E−03 | 1.11E−03 | 9.62E−03 | 4.05E−07 | 1.75E−03 | 3.34E−05 | 6.60E−04 | 5.81E−05 | 7.11E−04 | 8.16E−06 | 4.18E−04 |
| 2.91E+00 | 3.07E−03 | 1.11E−03 | 9.62E−03 | 4.05E−07 | 1.75E−03 | 3.34E−05 | 6.60E−04 | 5.81E−05 | 7.11E−04 | 8.16E−06 | 4.18E−04 |
| 2.87E+00 | 3.07E−03 | 1.11E−03 | 9.62E−03 | 4.05E−07 | 1.75E−03 | 3.34E−05 | 6.60E−04 | 5.81E−05 | 7.11E−04 | 8.16E−06 | 4.18E−04 |
| 2.83E+00 | 3.07E−03 | 1.11E−03 | 9.62E−03 | 4.04E−07 | 1.75E−03 | 3.34E−05 | 6.60E−04 | 5.81E−05 | 7.11E−04 | 8.16E−06 | 4.18E−04 |
| 2.78E+00 | 3.07E−03 | 1.11E−03 | 9.62E−03 | 3.65E−07 | 1.75E−03 | 3.34E−05 | 6.60E−04 | 5.81E−05 | 7.11E−04 | 8.16E−06 | 4.18E−04 |
| 2.74E+00 | 3.07E−03 | 1.11E−03 | 9.62E−03 | 2.94E−10 | 1.75E−03 | 3.34E−05 | 6.60E−04 | 5.81E−05 | 7.11E−04 | 8.16E−06 | 4.18E−04 |
| 2.69E+00 | 3.07E−03 | 1.11E−03 | 9.78E−03 | 1.74E−13 | 1.55E−03 | 3.34E−05 | 6.60E−04 | 5.81E−05 | 7.11E−04 | 8.15E−06 | 4.18E−04 |
| 2.65E+00 | 3.08E−03 | 1.10E−03 | 1.09E−02 | 1.32E−14 | 1.54E−04 | 3.34E−05 | 6.59E−04 | 5.81E−05 | 7.11E−04 | 8.10E−06 | 4.19E−04 |
| 2.61E+00 | 3.62E−03 | 4.79E−04 | 1.09E−02 | 7.39E−17 | 1.30E−04 | 3.34E−05 | 6.57E−04 | 5.79E−05 | 7.15E−04 | 4.82E−06 | 4.20E−04 |
| 2.56E+00 | 3.75E−03 | 4.63E−06 | 1.09E−02 | 1.15E−17 | 1.31E−04 | 3.18E−05 | 6.66E−04 | 4.89E−05 | 7.72E−04 | 2.81E−07 | 3.81E−04 |
| 2.52E+00 | 6.25E−04 | 4.80E−06 | 1.08E−02 | 1.06E−17 | 6.68E−05 | 1.31E−06 | 7.09E−04 | 5.15E−08 | 1.15E−03 | 7.81E−09 | 6.94E−05 |
| 2.48E+00 | 8.09E−05 | 2.23E−05 | 5.63E−03 | 1.33E−17 | 2.51E−07 | 1.18E−07 | 5.97E−04 | 2.82E−07 | 1.78E−03 | 1.03E−12 | 4.26E−09 |
| 2.43E+00 | 1.16E−07 | 5.10E−08 | 3.03E−06 | 5.19E−18 | 5.02E−09 | 3.45E−09 | 6.11E−06 | 7.99E−09 | 1.48E−05 | 1.55E−18 | 7.27E−19 |
| 2.39E+00 | 1.63E−25 | 4.58E−26 | 1.63E−24 | 9.50E−29 | 4.17E−27 | 3.98E−27 | 2.72E−24 | 7.78E−27 | 4.83E−24 | 3.90E−28 | 6.22E−28 |
| 2.35E+00 | 1.14E−19 | 3.34E−20 | 3.47E−19 | 1.62E−28 | 5.76E−22 | 6.59E−22 | 2.17E−19 | 4.83E−22 | 1.22E−19 | 3.90E−28 | 5.25E−28 |
| 2.30E+00 | 5.00E−29 | 5.40E−29 | 9.90E−29 | 9.50E−29 | 1.64E−28 | 2.07E−28 | 2.45E−28 | 2.65E−28 | 3.42E−28 | 3.90E−28 | 5.25E−28 |
| 2.26E+00 | 1.01E−27 | 5.40E−29 | 9.90E−29 | 9.50E−29 | 1.64E−28 | 2.07E−28 | 2.45E−28 | 2.65E−28 | 3.42E−28 | 3.90E−28 | 5.25E−28 |
| 2.21E+00 | 5.00E−29 | 5.40E−29 | 9.90E−29 | 9.50E−29 | 1.64E−28 | 2.07E−28 | 2.45E−28 | 2.65E−28 | 3.42E−28 | 3.90E−28 | 5.25E−28 |
| 2.17E+00 | 5.00E−29 | 5.40E−29 | 9.90E−29 | 9.50E−29 | 1.65E−28 | 2.07E−28 | 2.45E−28 | 2.65E−28 | 3.42E−28 | 3.90E−28 | 5.25E−28 |
| 2.13E+00 | 5.00E−29 | 5.40E−29 | 9.90E−29 | 9.50E−29 | 1.64E−28 | 2.07E−28 | 2.45E−28 | 2.65E−28 | 3.42E−28 | 3.90E−28 | 5.25E−28 |
| 2.08E+00 | 5.00E−29 | 5.40E−29 | 9.90E−29 | 9.50E−29 | 1.64E−28 | 2.07E−28 | 2.45E−28 | 2.65E−28 | 3.42E−28 | 3.90E−28 | 5.25E−28 |
| 2.04E+00 | 9.22E−28 | 5.63E−29 | 1.14E−28 | 9.50E−29 | 1.86E−19 | 2.07E−28 | 2.45E−28 | 2.65E−28 | 3.42E−28 | 3.90E−28 | 5.25E−28 |
| 2.00E+00 | 1.13E−26 | 2.58E−28 | 3.99E−28 | 9.50E−29 | 9.62E−18 | 2.07E−28 | 2.45E−28 | 2.65E−28 | 3.42E−28 | 3.90E−28 | 5.25E−28 |
| 1.95E+00 | 2.78E−26 | 6.13E−28 | 8.16E−28 | 9.50E−29 | 8.37E−17 | 2.07E−28 | 2.45E−28 | 2.65E−28 | 3.42E−28 | 3.90E−28 | 5.25E−28 |
| 1.91E+00 | 1.88E−19 | 2.57E−22 | 5.39E−07 | 9.50E−29 | 3.30E−16 | 2.07E−28 | 2.45E−28 | 2.65E−28 | 3.42E−28 | 3.90E−28 | 5.25E−28 |
| 1.87E+00 | 1.51E−19 | 6.95E−22 | 6.56E−07 | 3.07E−24 | 9.37E−16 | 3.81E−12 | 7.13E−22 | 7.44E−23 | 4.28E−22 | 1.15E−23 | 5.34E−23 |
| 1.82E+00 | 1.11E−19 | 3.53E−22 | 7.41E−07 | 2.48E−24 | 2.38E−15 | 2.65E−11 | 1.97E−22 | 2.10E−23 | 1.19E−22 | 3.26E−24 | 1.48E−23 |
| 1.78E+00 | 9.63E−20 | 3.38E−22 | 8.03E−07 | 1.02E−23 | 5.16E−15 | 2.50E−10 | 1.40E−22 | 1.51E−23 | 8.56E−23 | 2.44E−24 | 1.05E−23 |
| 1.73E+00 | 8.81E−20 | 3.14E−22 | 8.48E−07 | 1.03E−23 | 9.86E−15 | 3.93E−10 | 6.55E−23 | 7.18E−24 | 4.05E−23 | 1.22E−24 | 1.09E−10 |
| 1.69E+00 | 1.34E−19 | 1.07E−21 | 8.77E−07 | 1.91E−06 | 5.94E−13 | 5.79E−10 | 3.99E−23 | 4.42E−24 | 2.49E−23 | 8.01E−25 | 3.18E−10 |
| 1.65E+00 | 1.13E−19 | 9.44E−22 | 8.91E−07 | 2.26E−06 | 1.33E−12 | 8.43E−10 | 3.02E−23 | 3.38E−24 | 1.90E−23 | 6.67E−25 | 8.27E−10 |
| 1.60E+00 | 1.07E−19 | 8.98E−22 | 8.76E−07 | 2.56E−06 | 2.88E−12 | 1.09E−09 | 2.51E−23 | 2.84E−24 | 1.59E−23 | 5.82E−25 | 8.99E−10 |
| 1.56E+00 | 1.06E−19 | 9.20E−22 | 8.21E−07 | 2.84E−06 | 6.11E−12 | 1.33E−09 | 2.82E−23 | 3.20E−24 | 1.80E−23 | 3.43E−10 | 9.26E−10 |
| 1.52E+00 | 1.02E−19 | 9.56E−22 | 7.14E−07 | 3.12E−06 | 1.26E−11 | 1.53E−09 | 2.80E−23 | 3.20E−24 | 1.80E−23 | 4.15E−10 | 1.00E−09 |
| 1.47E+00 | 9.09E−20 | 9.51E−22 | 5.55E−07 | 3.38E−06 | 2.49E−11 | 1.63E−09 | 2.95E−23 | 3.39E−24 | 1.91E−23 | 4.86E−10 | 1.09E−09 |
| 1.43E+00 | 7.01E−20 | 8.24E−22 | 3.69E−07 | 3.62E−06 | 4.67E−11 | 1.55E−09 | 6.88E−24 | 7.95E−25 | 4.46E−24 | 5.52E−10 | 3.62E−10 |
| 1.38E+00 | 4.46E−20 | 6.05E−22 | 1.96E−07 | 3.84E−06 | 8.30E−11 | 1.27E−09 | 5.55E−24 | 6.43E−25 | 3.61E−24 | 6.10E−10 | 3.78E−10 |
| 1.34E+00 | 2.21E−20 | 3.51E−22 | 7.69E−08 | 3.96E−06 | 1.38E−10 | 8.03E−10 | 4.60E−24 | 5.35E−25 | 3.01E−24 | 5.70E−10 | 3.66E−10 |
| 1.30E+00 | 8.72E−21 | 1.68E−22 | 1.99E−08 | 4.17E−06 | 2.27E−10 | 4.00E−10 | 3.80E−24 | 4.42E−25 | 2.49E−24 | 6.87E−10 | 4.05E−10 |
| 1.25E+00 | 3.63E−21 | 8.34E−23 | 3.11E−09 | 4.29E−06 | 3.54E−10 | 1.29E−10 | 3.04E−24 | 3.54E−25 | 1.99E−24 | 7.21E−10 | 4.18E−10 |
| 1.21E+00 | 2.20E−21 | 5.41E−23 | 4.49E−10 | 4.20E−06 | 5.07E−10 | 2.43E−11 | 2.31E−24 | 2.69E−25 | 1.51E−24 | 5.48E−10 | 3.98E−10 |
| 1.17E+00 | 2.01E−21 | 4.98E−23 | 2.69E−10 | 4.41E−06 | 6.81E−10 | 6.58E−12 | 1.90E−24 | 2.23E−25 | 1.25E−24 | 7.88E−10 | 4.43E−10 |
| 1.12E+00 | 2.28E−21 | 5.64E−23 | 2.11E−10 | 4.41E−06 | 6.83E−10 | 7.48E−12 | 2.13E−24 | 2.49E−25 | 1.40E−24 | 7.89E−10 | 4.42E−10 |
| 1.08E+00 | 2.61E−21 | 6.46E−23 | 2.08E−10 | 4.41E−06 | 6.79E−10 | 8.77E−12 | 2.41E−24 | 2.82E−25 | 1.59E−24 | 7.89E−10 | 4.41E−10 |
| 1.04E+00 | 3.00E−21 | 7.42E−23 | 2.34E−10 | 4.41E−06 | 6.70E−10 | 1.07E−11 | 2.75E−24 | 3.22E−25 | 1.81E−24 | 7.89E−10 | 4.40E−10 |
| 9.92E−01 | 3.44E−21 | 8.52E−23 | 2.63E−10 | 4.41E−06 | 6.56E−10 | 1.36E−11 | 3.18E−24 | 3.71E−25 | 2.09E−24 | 7.90E−10 | 4.39E−10 |
| 9.48E−01 | 4.03E−21 | 9.94E−23 | 3.79E−10 | 4.42E−06 | 6.38E−10 | 2.03E−11 | 3.69E−24 | 4.31E−25 | 2.43E−24 | 7.90E−10 | 4.38E−10 |
| 9.05E−01 | 4.67E−21 | 1.15E−22 | 4.59E−10 | 4.42E−06 | 6.17E−10 | 2.62E−11 | 4.33E−24 | 5.05E−25 | 2.85E−24 | 7.90E−10 | 4.37E−10 |
| 8.61E−01 | 5.54E−21 | 1.36E−22 | 6.58E−10 | 4.42E−06 | 5.93E−10 | 3.56E−11 | 5.10E−24 | 5.96E−25 | 3.36E−24 | 7.90E−10 | 4.35E−10 |
| 8.17E−01 | 6.62E−21 | 1.61E−22 | 9.01E−10 | 4.42E−06 | 5.66E−10 | 4.62E−11 | 6.06E−24 | 7.06E−25 | 3.99E−24 | 7.90E−10 | 4.34E−10 |
| 7.74E−01 | 8.16E−21 | 1.97E−22 | 1.36E−09 | 4.43E−06 | 5.35E−10 | 6.21E−11 | 7.24E−24 | 8.45E−25 | 4.77E−24 | 7.90E−10 | 4.32E−10 |
| 7.30E−01 | 1.01E−20 | 2.41E−22 | 1.82E−09 | 4.43E−06 | 5.08E−10 | 7.97E−11 | 8.63E−24 | 1.01E−24 | 5.68E−24 | 7.90E−10 | 4.30E−10 |
| 6.87E−01 | 1.26E−20 | 3.00E−22 | 2.45E−09 | 4.43E−06 | 4.81E−10 | 1.02E−10 | 1.03E−23 | 1.20E−24 | 6.78E−24 | 7.91E−10 | 4.29E−10 |
| 6.43E−01 | 1.65E−20 | 3.88E−22 | 3.47E−09 | 4.43E−06 | 4.53E−10 | 1.33E−10 | 1.23E−23 | 1.44E−24 | 8.12E−24 | 7.91E−10 | 4.27E−10 |
| 5.99E−01 | 2.27E−20 | 5.27E−22 | 5.13E−09 | 4.43E−06 | 4.24E−10 | 1.73E−10 | 1.48E−23 | 1.72E−24 | 9.74E−24 | 7.91E−10 | 4.25E−10 |
| 5.56E−01 | 3.30E−20 | 7.52E−22 | 7.74E−09 | 4.44E−06 | 3.95E−10 | 2.24E−10 | 1.77E−23 | 2.07E−24 | 1.17E−23 | 7.91E−10 | 4.23E−10 |
| 5.12E−01 | 4.98E−20 | 1.12E−21 | 1.17E−08 | 4.44E−06 | 3.67E−10 | 2.88E−10 | 2.13E−23 | 2.48E−24 | 1.40E−23 | 7.91E−10 | 4.21E−10 |
| 4.68E−01 | 7.55E−20 | 1.68E−21 | 1.71E−08 | 4.44E−06 | 3.39E−10 | 3.67E−10 | 2.56E−23 | 2.98E−24 | 1.69E−23 | 7.91E−10 | 4.19E−10 |
| 4.25E−01 | 1.15E−19 | 2.55E−21 | 2.43E−08 | 4.44E−06 | 3.11E−10 | 4.64E−10 | 3.08E−23 | 3.59E−24 | 2.03E−23 | 7.91E−10 | 4.17E−10 |
| 3.81E−01 | 1.79E−19 | 3.92E−21 | 3.45E−08 | 4.44E−06 | 2.85E−10 | 5.80E−10 | 3.70E−23 | 4.31E−24 | 2.44E−23 | 7.91E−10 | 4.14E−10 |
| 3.37E−01 | 2.79E−19 | 6.09E−21 | 4.86E−08 | 4.45E−06 | 2.60E−10 | 7.20E−10 | 4.46E−23 | 5.20E−24 | 2.94E−23 | 7.91E−10 | 4.12E−10 |
| 2.94E−01 | 4.37E−19 | 9.52E−21 | 6.77E−08 | 4.45E−06 | 2.36E−10 | 8.85E−10 | 5.39E−23 | 6.28E−24 | 3.55E−23 | 7.91E−10 | 4.10E−10 |
| 2.50E−01 | 6.86E−19 | 1.49E−20 | 9.31E−08 | 4.45E−06 | 2.13E−10 | 1.08E−09 | 6.54E−23 | 7.62E−24 | 4.31E−23 | 7.91E−10 | 4.08E−10 |
| 2.06E−01 | 1.08E−18 | 2.34E−20 | 1.26E−07 | 4.45E−06 | 1.91E−10 | 1.31E−09 | 7.99E−23 | 9.31E−24 | 5.27E−23 | 7.91E−10 | 4.06E−10 |
| 1.63E−01 | 1.72E−18 | 3.71E−20 | 1.70E−07 | 4.45E−06 | 1.71E−10 | 1.57E−09 | 9.90E−23 | 1.15E−23 | 6.52E−23 | 7.91E−10 | 4.04E−10 |
| 1.19E−01 | 2.80E−18 | 6.05E−20 | 2.30E−07 | 4.45E−06 | 1.51E−10 | 1.89E−09 | 1.26E−22 | 1.46E−23 | 8.27E−23 | 7.91E−10 | 4.02E−10 |
| 7.54E−02 | 4.88E−18 | 1.05E−19 | 3.14E−07 | 4.46E−06 | 1.33E−10 | 2.30E−09 | 1.68E−22 | 1.96E−23 | 1.11E−22 | 7.91E−10 | 3.99E−10 |

The equation of state is one more relation as follows:

$$p_{\rm gas} = k(T_{\rm i}/\mu_{\rm i} + T_{\rm e}/\mu_{\rm e})/m_{\rm u}, \tag{6}$$

where $\mu$ denotes the mean molecular weight, $k$ denotes Boltzmann's constant, and $m_{\rm u}$ denotes the atomic mass unit.

Therefore, we have obtained a group of six equations consisting of one integral, two algebraic, and three differential equations, i.e., Eqs. (1)–(6) for six unknown quantities, $H$ (or $c_{\rm s}$), $v$, $\rho$, $\Omega$, $T_{\rm i}$ and $T_{\rm e}$. This group of equations can be calculated under three outer boundary conditions with some specialized parameters, which will be given in the following.

It should be noted that we ignore the outflow for simplicity as the first estimation, which means that our results are the upper limit. Therefore, we consider a stellar mass black hole ($10M_{\odot}$) and choose mass accretion rate of $10^{-2}\dot{M}_{\rm E}$ ($\dot{M}_{\rm E}$ denotes the Eddington accretion rate). In units of the Schwarzschild gravitational radius, the calculated results are presented in Fig. 1, which demonstrates densities and temperatures of solution of ADAF as a function of radius. It can be seen that the temperature and density clearly decrease with the increasing radius, different from that of Hu *et al.*[12]

At any given time, a traditional nuclear reaction network code including reaction rates[14,15] employed in this study contains about 500 relevant isotopes from light through heavy, such as hydrogen, helium, deuterium, up to $^{91}$Tc. It is well known that the nuclear reaction networks include a set of adjoined ordinary differential equations, and mass fractions of isotopes change over time associated the process of the global solutions of the ADAF. Similar to the hypothesis of Hu *et al.*,[12] we also postulate that the nuclear burning is hydrostatic, namely, constant temperature and density ($dT/dt = 0$ and $d\rho/dt = 0$). Without loss of generality, solar abundances is adopted as the initial composition. In addition, the temperature is in units of kelvin and density is in gram per cubic centimeter. We calculate nucleosynthesis in ADAF and obtain the mass fractions of various isotopes using nuclear reaction network. Our goal is concerned with the abundances of light isotopes and the calculated results are shown in Figs. 2 and 3 and Table 1.

Heatmaps in Figs. 2 and 3 show the variation characteristics of different isotopes, when the material is accreted onto a black hole. The horizontal axis is mass fractions ($10^{-28}$–$10^{-3}$) of isotopes from $^{11}$C to $^{42}$S in logarithmic units and the vertical axis denotes the radial coordinates set in the Schwarzschild gravitational units. Colors in each zone of the heatmap present the mass fraction of a given radius. Zones deeper to red show the higher abundances in the nucleosynthesis in ADAF onto a black hole.

Figures 2 and 3 illustrate that some isotopic abundances may present abnormal patterns due to nucleosynthesis in ADAF onto a black hole. In particular, supersolar metal abundance is one of the most important probes for nucleosynthesis in ADAF around the galactic center or the afterglow of the gamma-ray burst (GRB). Savaglio *et al.*[16] have detected the abnormally high metallicity observed at high redshift with the very large telescope spectrum of GRB. Moreover, on account of hot temperature, the abundance of protons may influence the gamma-ray spectrum originated from the proton–proton collisions and $\pi^0$ decay.[17] In addition, it should be noted that the current instruments cannot measure the spectra of isotopes in ADAF onto a black hole, which requires the more powerful equipments.

It is important to note that the ultimate mass fractions of some nuclides display significantly high (for example, $^6$Li even as high as $\sim 10^{-5}$ near black hole). Although researchers still do not obtain the observed isotopic abundance of the nucleosynthesis sites of black hole accretion disks, from the calculated results it can be predicted that the abundances of some isotopes should present supersolar metal abundances, probably revealed by the spectrum of ADAF onto black hole in the future.

It is well known that self-similar solutions of ADAF would lead to a significant uncertainty in the hot accretion disks and outflow regions.[18] Therefore, based on the global solution of ADAFs, we revisit nucleosynthesis mechanism in accretion disks around black holes. It is found that our simulation results show a predicted isotopic abundance to the observations from high-resolution spectroscopic data. In a sense, this means the intrinsic nucleosynthesis characteristic in the chemical evolution of black hole accretion disks. Obviously, to test this hypothesis, further accurate spectrum observation of accretion disks around compact stars is desired, which will initiate the new clue of chemical evolution and nucleosynthesis in the early galaxy.[19,20]

We thank Qiu-He Peng, Zhan-Wen Han and F X Timmes for their kind assistance in this work.

## References

[1] Burbidge M, Burbidge G R, Fowler W and Hoyle F 1957 *Rev. Mod. Phys.* **29** 547
[2] Busso M, Gallino R and Wasserburg G J 1999 *Annu. Rev. Astron. Astrophys.* **37** 239
[3] Arnould M, Goriely S and Takahashi K 2007 *Phys. Rep.* **450** 97
[4] Han Z and Podsiadlowski Ph 2004 *Mon. Not. R. Astron. Soc.* **350** 1301
[5] Wang B and Han Z 2012 *New Astron. Rev.* **56** 122
[6] Shakura N I and Sunyaev R A 1973 *Astron. Astrophys.* **24** 337
[7] Narayan R and Yi I 1994 *Astrophys. J.* **428** L13
[8] Narayan R, Kato S and Honma F 1997 *Astrophys. J.* **476** 49
[9] Banerjee I and Mukhopadhyay B 2013 *Astrophys. J.* **778** 8
[10] Mukhopadhyay B and Chakrabarti S K 2000 *Astron. Astrophys.* **353** 1029
[11] Surman R McLaughlin G C and Sabbatino N 2011 *Astrophys. J.* **743** 155
[12] Hu T and Peng Q H 2008 *Astrophys. J.* **681** 96
[13] Yuan F, Quataert E and Narayan R 2003 *Astrophys. J.* **598** 301
[14] Timmes F X 1999 *Astrophys. J. Suppl. Ser.* **124** 241
[15] Timmes F X, Hoffman R D and Woosley S E 2000 *Astrophys. J. Suppl. Ser.* **129** 377
[16] Savaglio S, Rau A, Greiner J et al 2012 *Mon. Not. R. Astron. Soc.* **420** 627
[17] Xu Y D and Cao X 2010 *Astrophys. J.* **716** 1423
[18] Zhang H, Wang Y, Yuan F, Ding F, Luo X and Peng Q H 2009 *Astron. Astrophys.* **502** 419
[19] Zhang J, Wang B, Zhang B and Han Z 2012 *Chin. Phys. Lett.* **29** 019701
[20] Wang J T and Song H F 2016 *Chin. Phys. Lett.* **33** 099702